PHYSICAL REVIEW B VOLUME 22, NUMBER 4 15 AUGUST 1980

Neutron scattering study on the kinetics of clustering in CuNi alloys

J. Vrijen,* J. Aalders, and C. van Dijk
Netherlands Energy Research Foundation ECN, Petten (N.H.), The Netherlands

S. Radelaar
Laboratory of Metallurgy, Delft University of Technology, Rotterdamseweg 137, Delft, The Netherlands

(Received 26 November 1979)

This paper describes an investigation of the kinetics of clustering (preference for like nearest neighbors) in a number of CuNi alloys. The kinetics was studied by measuring the evolution of the diffuse neutron-scattering cross section with time. In order to maximize the diffuse scattering, the isotopes ^{62}Ni and ^{65}Cu were used. The experimental results are compared with a theoretical model based on the lattice diffusion theory of spinodal decomposition. Good agreement is obtained for long-wavelength composition fluctuations. For short wavelengths agreement is not quite satisfactory. Values of thermodynamic and kinetic parameters deduced from the experiments are in good agreement with data obtained with different techniques at high temperatures.

I. INTRODUCTION

In an earlier paper[1] one of the authors discussed the kinetics of short-range order (SRO) in ordering alloy systems by calculating the time dependence of the first shell correlation coefficient. Nearest-neighbor interactions and a vacancy diffusion model for the atomic transport were used. In this way a relation was found between the relaxation time for SRO and the diffusion coefficients of the components of the alloy. A single relaxation time appeared to be a reasonable approximation for SRO and this has been verified experimentally.[2,3] Cook[4] showed that in contrast to short-range-order kinetics, clustering kinetics cannot be described, even approximately, by a single relaxation time. Similar results on diffusion on an atomic scale in binary and multicomponent alloys were derived by Khachaturyan.[5,6] Recently, Yamauchi[7] developed an interesting statistical mechanical model for the time evolution of the pair-correlation function for discrete lattices. The results of his model agree with those of Cook's model as far as long-range correlations are concerned, but the predictions of both models concerning the time evolution of the pair correlations over short distances differ. According to Cook[8] the model for describing the kinetics of clustering in stable solid solutions is the discrete lattice analog[9] of the continuum model for the early stages of spinodal decomposition as developed by Cahn.[10-14] So the formalism of describing clustering kinetics in the stable single phase above the critical temperature for decomposition is basically the same as that for describing the decomposition behavior in the unstable region below T_c. However, the former case is far less complicated since the diffusion equation for the single phase can be linearized at all stages of the relaxation process. This does not hold for the unstable regime where nonlinearities complicate the mathematical treatment tremendously.[13,15-18] Consequently, an experimental study of clustering kinetics provides an opportunity of verifying experimentally the mechanism that governs the very early stages of spinodal decomposition. Until now no quantitative experimental data on clustering kinetics were available, at least not to our knowledge. Earlier work showed that changes in the electrical resistivity of clustering systems during relaxation towards equilibrium could not be described with a single relaxation time.[19] However, electrical resistivity measurements, despite the very high sensitivity of the technique, are not suited to investigate the time evolution of the pair correlations in clustering systems since the various composition wavelengths produce a different contribution to the electron scattering. Diffuse scattering of x-rays or thermal neutrons is probably the only method that gives sufficiently accurate information on the atomic configurations for a worthwhile comparison of clustering and clustering kinetics in real systems with the various models that have been developed.

The system Cu-Ni has been chosen for the following reasons: (i) the system exhibits complete solid solubility over a wide temperature range, (ii) the atomic mobility allows equilibrium states of the system to be reached in an easily accessible temperature range, and (iii) it is one of the systems best suited for diffuse-scattering experiments when investigated with thermal neutrons, particularly if the isotopes ^{65}Cu and ^{62}Ni are used. The equilibrium clustering in this system has been discussed in detail elsewhere.[20-22]

II. THEORY

Hitherto the problem of the equilibrium atomic distribution over the lattice sites in binary alloys has not been solved exactly. Therefore, it is not surprising that no exact solution for the kinetic problem, which is even more complicated, has been found either. Various theories have been developed from different points of view for the description of these nonequilibrium processes. Important theoretical progress was achieved by Cahn's introduction of the concept of spinodal decomposition. Using an expansion of the free energy as a function of concentration he was able to solve the diffusion equation which describes the atomic transport in nonequilibrium.

In general, the time-dependent atomic distribution $c(\vec{r},t)$, describing the composition on site $\vec{r}$ at time t, can be expressed as a Fourier series

$$c(\vec{r},t)-c_0=\sum_{\vec{\kappa}} A(\vec{\kappa},t)e^{i\vec{\kappa}\cdot\vec{r}}\,, \tag{2.1}$$

where $\vec{\kappa}$ is a wave vector. Cahn considers only an elastic continuum where $\vec{r}$ is a continuous parameter. For the time-dependent behavior of $A(\vec{\kappa},t)$ he derived

$$A(\vec{\kappa},t)=A(\vec{\kappa},0)e^{R(\vec{\kappa})t}\,, \tag{2.2}$$

where the amplification factor $R(\vec{\kappa})$ is given by

$$R(\vec{\kappa})=-M\kappa^2(f''+2\eta^2Y+2K\kappa^2)\,, \tag{2.3}$$

where M is the atomic mobility, f'' is the second derivative of the Helmholtz free energy with respect to the composition, η is the linear strain per unit composition difference, Y is the effective elastic modulus, and K is the gradient-energy coefficient.

Equation (2.3) shows that inside the coherent spinodal ($f''+2\eta^2Y\leq 0$), depending on the sign of $R(\vec{\kappa})$, certain composition fluctuations decay and others grow in time. This is shown in Fig. 1. It is also shown that for temperatures above the miscibility gap all composition fluctuations should decay, all with different relaxation times, depending on $\vec{\kappa}$. This would mean that above the critical temperature the distribution of the atoms over the available lattice sites is random since in Cahn's theory fluctuations are neglected. This is in contradiction with numerous experiments, e.g.,[22] where it is found that composition fluctuations occur above the critical temperature. Furthermore, because of the continuum description, Cahn's theory is only correct for Fourier components with wavelengths long compared to the lattice spacing. For these reasons Cook, de Fontaine, and Hilliard generalized Cahn's ideas by describing the diffusion on a discrete lattice.[9] Instead of Eq. (2.2) they derived

$$A(\vec{\kappa},t)=A(\vec{\kappa},0)e^{a(\vec{\kappa})t}\,, \tag{2.4}$$

where

$$a(\vec{\kappa})=-MB^2(\vec{\kappa})[f''+2\eta^2Y+2KB^2(\vec{\kappa})]\,. \tag{2.5}$$

Note that in this expression for the amplification factor, the factor $B^2(\vec{\kappa})$ instead of κ^2 occurs. $B^2(\vec{\kappa})$ represents a lattice sum, and for a cubic system is defined by

$$B^2(\vec{\kappa})=\left(\frac{1}{a_0^2}\right)\sum_{r}{}' [1-\cos(\vec{\kappa}\cdot\vec{r})]\,, \tag{2.6}$$

where a_0 is the lattice parameter and the suffix indicates that the summation runs only over nearest-neighbor positions. For small values of κ it is acceptable to replace $B^2(\vec{\kappa})$ by κ^2, which reduces Cahn's model to a special case of the generalized model of Cook, de Fontaine, and Hilliard.

The discrete lattice diffusion model extends the validity range to all possible Fourier components and should be an improvement on Cahn's model for $\vec{\kappa}>0.6$ Å^{-1}. A comparison of $a(\vec{\kappa})$ and $R(\vec{\kappa})$ for an fcc lattice with $a_0\simeq 3.5$ Å is shown in Fig. 2. Moreover, Cook[4] derived an expression for the time evolution of the diffuse-scattering cross section for x-rays, electrons, or thermal neutrons, which also takes into account the composition fluctuations above T_c:

$$\frac{d\sigma}{d\Omega}(\vec{\kappa},t)_{\rm diff}=\left(\frac{d\sigma}{d\Omega}(\vec{\kappa},0)-\frac{d\sigma}{d\Omega}(\vec{\kappa},\infty)\right)_{\rm diff}\exp[2a(\vec{\kappa})t]$$
$$+\frac{d\sigma}{d\Omega}(\vec{\kappa},\infty)_{\rm diff}\,. \tag{2.7}$$

This expression can be used for the early stages of spinodal decomposition [$a(\vec{\kappa})>0$] Ref. 8, as well as for the kinetics of both clustering and SRO [$a(\vec{\kappa})<0$] Ref. 4. With the help of Eq. (2.7) the deviations from Cahn's model as observed in de-

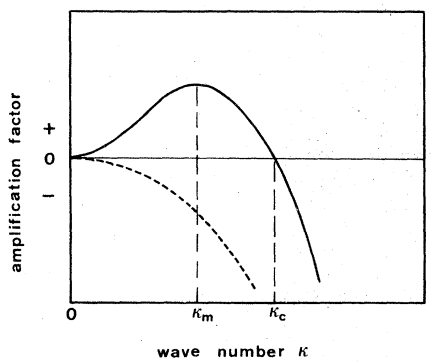

FIG. 1. Cahn's amplification factor $R(\vec{\kappa})$ versus the wave vector $\vec{\kappa}$ for a temperature inside (solid line) and outside the spinodal region (broken line).

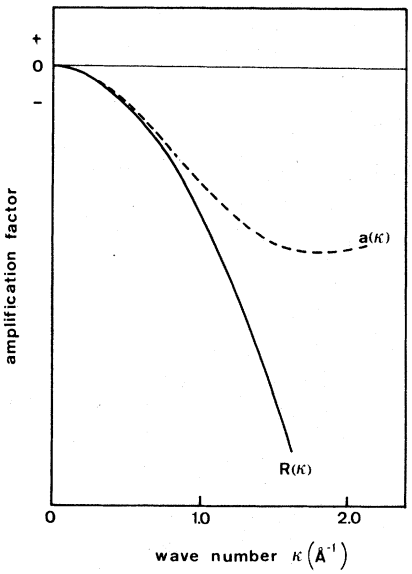

FIG. 2. Cahn's amplification factor $R(\kappa)$ and Cook's amplification factor $a(\kappa)$ for a polycrystalline fcc sample with $a_0 \simeq 3.5$ Å for a temperature outside the unstable region.

composing glasses by Neilson[23] and in Al-Zn by Acuña and Bonfiglioli[24] can be explained.

As is shown by Eq. (2.5), measurements of $a(\vec{\kappa})$ can give information on the mobility M, provided one has additional information on the thermodynamic driving force (the term between brackets). Statistical models exist which directly correlate the free energy with the Warren-Cowley parameters. However, we prefer a different approach.

According to fluctuation theory the diffuse scattering for N scatterers in a volume V will be given by[25]

$$\frac{d\sigma}{d\Omega}(\vec{\kappa},\infty)=N(b_A-b_B)^2\,\frac{k_BT}{V[f''+2\eta^2Y+2KB^2(\vec{\kappa})]}\,. \tag{2.8}$$

For small κ, $B^2(\vec{\kappa})$ can be replaced by κ^2. For $\kappa = 0$, Eq. (2.8) becomes

$$\frac{d\sigma}{d\Omega}(0,\infty)=\frac{N}{V}(b_A-b_B)^2\frac{k_BT}{f''+2\eta^2Y}\,.$$

Substitution of this expression yields (for small κ)

$$\frac{d\sigma}{d\Omega}(\vec{\kappa},\infty)=\frac{d\sigma}{d\Omega}(0,\infty)\frac{\kappa_c^2}{\kappa_c^2-\kappa^2}\,, \tag{2.9}$$

with

$$\kappa_c^2=-(f''+2\eta^2Y)/2K.$$

Measurements of the κ dependence of the diffuse scattering of an alloy in thermodynamic equilibrium enables one to determine κ_c^2 and hence the ratio of the second derivative of the free energy (including the elastic-energy term) and the gradient-energy coefficient.

III. EXPERIMENTAL PROCEDURE

Cu and Ni have almost the same number of electrons. Therefore the scattering factors for x-rays of Cu and Ni are nearly the same ($|f_{Cu}-f_{Ni}|/f_{Cu} \sim 0.03$). For the scattering of thermal neutrons the ratio of scattering lengths for natural isotopic mixtures is much larger ($|b_{Cu}-b_{Ni}|/b_{Cu} \sim 0.36$). Natural Ni consists of several stable isotopes, each with a different scattering length. ^{62}Ni has a large negative scattering length ($b_{^{62}Ni} = -0.87\times10^{-12}$ cm). Using this isotope in combination with ^{65}Cu, which has the largest positive scattering length of the stable Cu isotopes ($b_{^{65}Cu} = 1.11\times10^{-12}$ cm), enormously increases the factor $|b_{Cu}-b_{Ni}|^2$, which determines the amount of diffuse scattering [see Eq. (2.8)]. Since the scattering lengths are of opposite sign, the Bragg contribution decreases when these isotopes are alloyed. The alloy with 56.5 at.% ^{62}Ni has no Bragg reflections at all since the average scattering length $c_{Cu}b_{Cu}+c_{Ni}b_{Ni}=0$ at that composition. For this reason it is called the null matrix. In addition, the isotopic incoherence is diminished by using highly pure ^{65}Cu and ^{62}Ni.

The isotopes were purchased from Oak Ridge National Laboratories. The materials specification is given in Table I. For an optimum use of the limited quantities of isotopes available, a procedure was followed by which the alloys were prepared two by two, starting at the extreme ends of the composition range of interest. After the measurements the specimens were used to produce two other compositions which were closer to each other. Details have been given elsewhere.[20,22] In this way a large part of the Cu-Ni system could be investigated with a minimum amount of material. Only polycrystalline samples have been examined.

All scattering experiments have been carried out at room temperature. Therefore all specimens had to be quenched fast enough to prevent noticeable changes in the atomic distribution during the quench. By quenching in water, a quench rate of approximately 10^4 °C s^{-1} for a specimen thickness of about 1 mm can be realized. Therefore only atomic distributions for temperatures at which the effective atomic jump frequency was less than about 2×10^2 jumps s^{-1} could be frozen in. This jump frequency slows down exponentially with decreasing temperature. Since temperatures at which annealing times of more than one month are required to attain equilibrium are obviously impractical, only a small temperature region is accessible in this way. Andries *et al.*[26] investigated these effects in detail, using the electrical resist-

TABLE I. Isotopical and chemical specification of the ^{62}Ni and ^{65}Cu purchased from Oak Ridge National Laboratories.

Batch No.	Amount (g)	^{58}Ni	^{60}Ni	^{61}Ni	^{62}Ni at. %	^{64}Ni	^{63}Cu	^{65}Cu	Most important chemical impurities (ppm)	
1	6	0.98(1)	0.82(1)	0.12(1)	97.94(3)	0.14(1)			Cu	200
									Fe	200
									Cr	<200
									Zn	<500
2	10	0.32(5)	0.63(5)	0.13(3)	98.83(10)	0.09(3)			Cu, Fe	<200
									Cr	<500
									Zn	<2000
3	15						0.31(3)	99.69(3)	Fe	<200
									Ni, Cr	<500
									Zn	<2000

ivity as a parameter for the amount of SRO. Using data of Van Royen *et al.*,[19] who investigated the kinetics of clustering in Cu-Ni alloys by means of resistivity measurements, we calculated that the temperature region between 340 and 700 °C was experimentally accessible. This was confirmed by a check on the sample with 70 at.% ^{62}Ni as shown in Fig. 3.

Nearly all neutron-scattering data were collected by means of one of the neutron spectrometers at the High Flux Reactor (HFR) at Petten. Soller slits with a horizontal divergence of 30 and 40 min of arc and in some cases of 20 and 40 min of arc were used between monochromator and specimen and between specimen and BF_3 counter, respectively. A focusing pyrolytic graphite monochromator was used to obtain the desired wavelength. When necessary, a pyrolytic graphite filter was used to suppress higher-order neutrons of wavelengths $\lambda_n = \lambda_0/n$ to less than 1%.[27] Flux variations were accounted for by a preset monitor in the incident neutron beam. All measurements

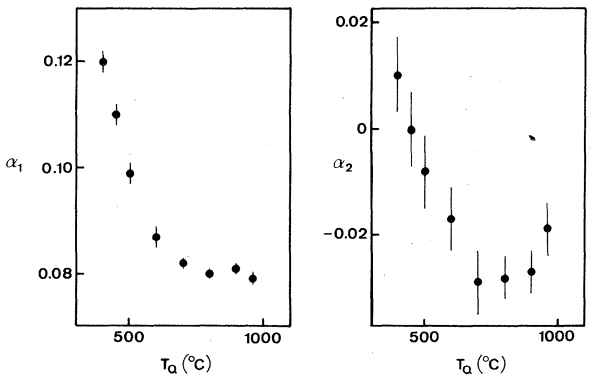

FIG. 3. The effect of the quench temperature on the cluster parameters α_1 and α_2 in $^{65}Cu_{0.30}$ $^{62}Ni_{0.70}$ for quenching in water ($\dot{T} \sim 10^4$ °C s^{-1}).

consisted of several runs in order to decrease experimental uncertainties. These runs were compared with each other and added to give the final data.

The small-κ data of the diffuse scattering were obtained by means of the small-angle neutron spectrometer (SANS) at Jülich. Extensive descriptions of this type of spectrometer have been published.[28,29] Via totally reflecting guide tubes, the SANS at Jülich obtains neutrons of very long wavelengths ($4.3 < \lambda < 10$ Å) from a cold source at the reactor FRJ-2. This, combined with the possibility of varying the distance between specimen and counterbank from 1 to 17 m, permits measurements at very small κ values of $4 \times 10^{-4} < \kappa < 0.2$ Å^{-1}. The counterbank consisted of five position-sensitive proportional BF_3 counters, each of which was divided into 64 channels. These counters were placed parallel to and above each other. The data are stored in the memory of a dedicated PDP-8 computer with a display screen. Collimation takes place by circular holes of variable diameter in cadmium plates at suitable positions along the beam path.

For the measurements at Petten the contribution of fast neutrons is by no means negligible. The background correction for the symmetric scattering arrangement is given by

$$\left.\frac{d\sigma}{d\Omega}\right|_{\text{corr}} = e^{\tau(s-1)}(I_p - I_{p+\text{Cd}}) - e^{-\tau}(I_H - I_{H+\text{Cd}}), \tag{3.1}$$

where $s = 1/\cos\theta$ (2θ is the scattering angle), $e^{-\tau}$ is the transmission of the specimen, while the subscripts p, $p+\text{Cd}$, H, and $H+\text{Cd}$ of the intensity I refer to specimen, specimen covered with cadmium, empty sample holder, and empty sample holder covered with cadmium, respectively. Equation (3.1) has been checked by measuring the in-

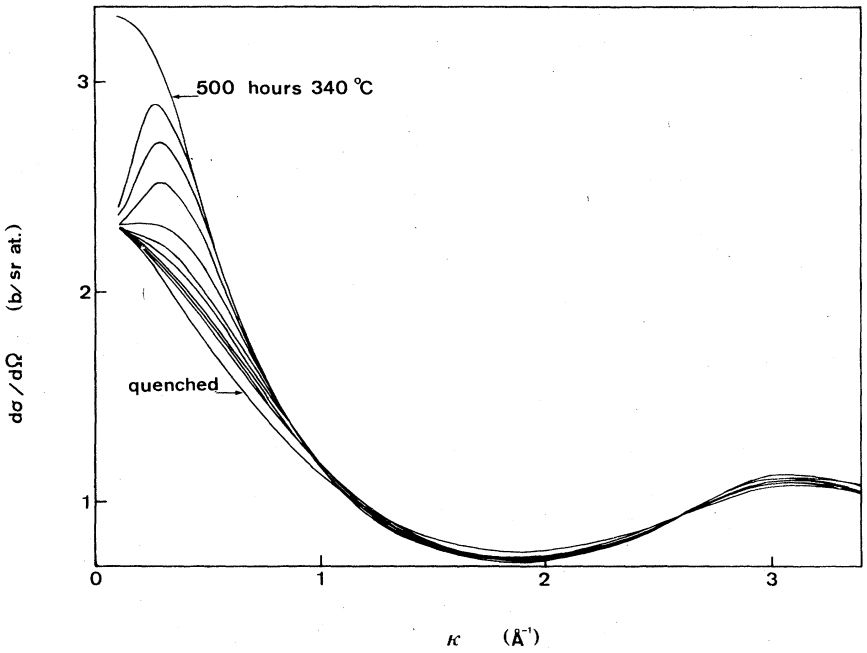

FIG. 4. Set of diffraction patterns showing the relaxation of the null matrix at 340 °C after 0, $\frac{1}{2}$, 1, 2, 5, 10, 20, 50, 100, 150, and 500 h, respectively.

coherent scattering of a thin vanadium sample in the specimen holder. The measurements were put on an absolute scale by comparison with the incoherent scattering from vanadium.

IV. EXPERIMENTAL RESULTS

For nine ^{65}Cu-^{62}Ni samples varying in composition between 20 and 80 at.% Ni, the time evolution of the diffuse scattering cross section for thermal neutrons at 400 °C has been measured. For the null matrix this time evolution has also been measured at 320, 340 (Fig. 4), 425, and 450 °C. All specimens were quenched from 700 °C. Subsequently they were annealed at the desired temperature for periods ranging from 5 min to 500 h. For all samples the κ range between 0.1 and 3.4 Å^{-1} was investigated at the reactor HFR at Petten. For the relaxation of the null matrix at 450 °C, the κ range between 0.01 and 0.2 Å^{-1} has also been investigated with 7.3-Å neutrons, using the small-angle neutron spectrometer of the Kernforschungsanlage (KFA) at Jülich. It appeared[20,22] that for the sample with 20 at.% Ni the differences in the amount of clustering between 400 and 700 °C were very small. For the other eight samples the successive changes in $d\sigma/d\Omega$ were large enough for quantitative evalua-

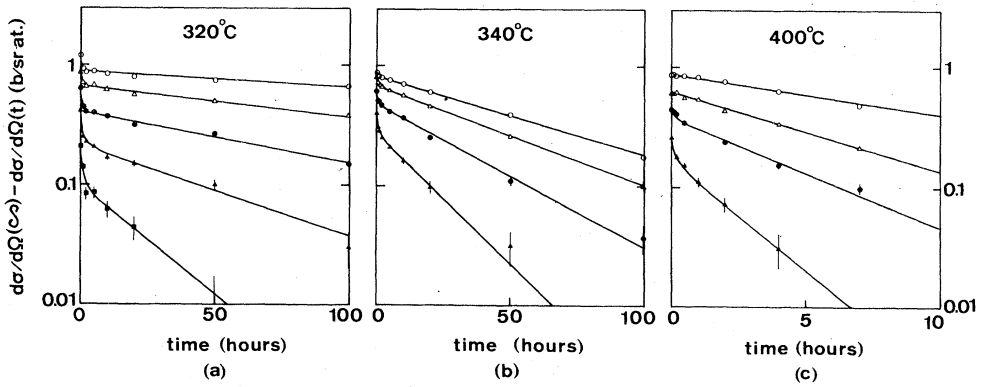

FIG. 5. Relaxation of the diffuse scattering cross section of the null matrix at 320 (a), 340 (b), and 400 °C (c); $\ln[d\sigma(\infty)/d\Omega - d\sigma(t)/d\Omega]$ plotted versus time for a few values of κ. ○: $\kappa = 0.3$ Å^{-1}; △: $\kappa = 0.4$ Å^{-1}; ●: $\kappa = 0.5$ Å^{-1}; ▲: $\kappa = 0.6$ Å^{-1}; ■: $\kappa = 0.7$ Å^{-1}. The solid lines are guided through the experimental points.

tion. The logarithm of the difference $d\sigma(\vec{\kappa},\infty)/d\Omega - d\sigma(\vec{\kappa},t)/d\Omega$ for a few relaxations of the null matrix have been plotted versus time in Fig. 5 for some values of κ. For a process which can be described with a single relaxation constant, the time dependence is represented by a straight line. Apart from deviations in the initial stages of the relaxations, which are most pronounced at the lower temperatures, the plots show a linear behavior with a different slope for each κ value. From these slopes the corresponding relaxation function $\tau(\vec{\kappa})$ has been deduced according to

$$\tau(\vec{\kappa}) = -[2a(\vec{\kappa})]^{-1} = t/\ln\left(\frac{d\sigma(\vec{\kappa},\infty)/d\Omega - d\sigma(\vec{\kappa},0)/d\Omega}{d\sigma(\vec{\kappa},\infty)/d\Omega - d\sigma(\vec{\kappa},t)/d\Omega}\right). \tag{4.1}$$

For κ values below 0.2 Å^{-1}, equilibrium could not be obtained at 450 °C. We therefore extrapolated the measured equilibrium data to $\kappa < 0.2$ Å^{-1} to obtain $(d\sigma/d\Omega)(\vec{\kappa},\infty)$.

The deviations from linear behavior in the initial stages of the relaxation process are due to a changing vacancy concentration during the relaxation. The excess vacancies, frozen in by quenching from 700 °C, disappear during the first annealing steps. In these early stages the vacancy supersaturation enhances diffusion and consequently the rate of relaxation.

For all relaxations at 400 °C and for those of the null matrix at 425 and 450 °C, the relative error in $\Delta(d\sigma/d\Omega)$ for $\kappa > 0.8$ Å^{-1} is of the order of 30% or more. This and the fact that in nearly all re-

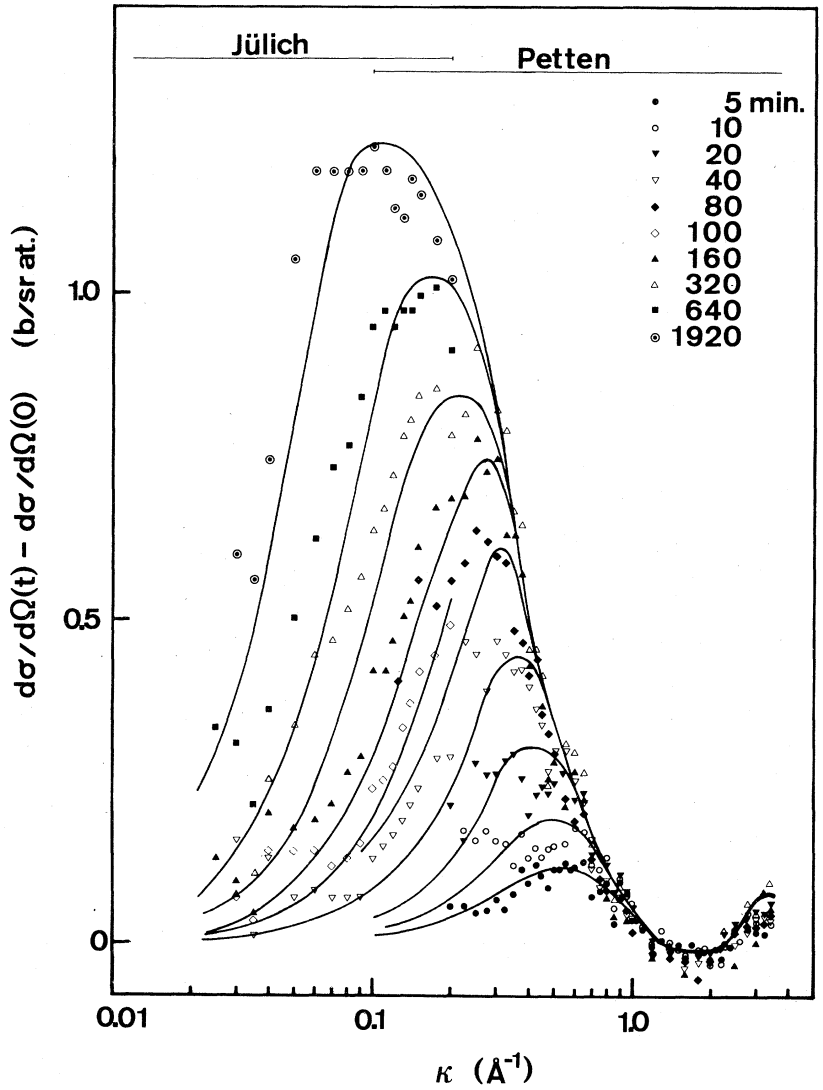

FIG. 6. The various stages of the relaxation of the null matrix at 450 °C as measured at Petten and at Jülich, together with the corresponding predictions of the model by Cook (solid lines).

laxations the first annealing step is about 5 times the shortest relaxation time involved (~50 s) make the data for $\tau(\vec{\kappa})$ in this κ-range rather unreliable. For low κ values, $\kappa < 0.2$ Å^{-1}, in most relaxations equilibrium could not be obtained owing to the very long annealing times needed there (Fig. 6). For these reasons only the data at κ values ranging from 0.2 to 0.8 Å^{-1} were used to fit Cook's model, using the expression

$$\tau^{-1}(\kappa) = -2a(\kappa) = A_1\left(1 - \frac{\sin\kappa r_1}{\kappa r_1}\right) + A_2\left(1 - \frac{\sin\kappa r_1}{\kappa r_1}\right)^2, \quad (4.2)$$

which is a spherical average of Eq. (2.5) for polycrystalline samples. A_1 and A_2 are constants for a specific relaxation and are used as parameters for the fitting procedure. In Cook's model these constants are given by

$$A_1 = 12\Omega c_{Ni} c_{Cu} \tilde{D}(f'' + 2\eta^2 Y)/(r_1^2 k_B T) \quad (4.3)$$

and

$$A_2 = 144\Omega c_{Ni} c_{Cu} \tilde{D} K/(r_1^4 k_B T)\,. \quad (4.4)$$

Ω is the specific atomic volume and r_1 is the nearest-neighbor distance. $\tilde{D}$ is the chemical diffusion coefficient for the relaxation process; in Cook's model it is defined by

$$\tilde{D} = c_{Ni} D_{Cu} + c_{Cu} D_{Ni}\,, \quad (4.5)$$

where D_{Cu} and D_{Ni} are the tracer diffusion coefficients of Cu and Ni, respectively, at that composition.

The parameters A_1 and A_2 for the relaxations at 400 °C are given in Table II and those for the relaxations of the null matrix at the various temperatures are given in Table III. For the relaxation of the null matrix at 450 °C the extrapolation of $\tau(\kappa)$ obtained in this way to κ values smaller than 0.2 Å^{-1} agrees extremely well with the results of the small-angle measurements carried out at Jülich (Fig. 7).

V. DISCUSSION

As is evident from Fig. 7 the agreement between the relaxation time calculated from Cook's theory and experimental values is excellent for values of κ below 0.8 Å^{-1}. Cook's model does not correctly describe the behavior around the crossover point, since, as we pointed out above, Cook assumed that the different composition waves grow or decay independently and moreover fluctuate independently. Hence, Cook's theory predicts that the diffuse intensity does not change with time for a certain value of κ (the crossover point). Since the total diffuse intensity is a conserved quantity during the relaxation experiment, an increase of the intensity at small κ must be accompanied by a corresponding decrease at large κ values. The consequences of this is that the crossover point will shift to lower κ values during relaxation as is demonstrated by Fig. 8. In the κ region where the crossover point is shifting, it is not possible to obtain reliable values for the relaxation times.

For $\kappa > 1.3$ Å^{-1} the uncertainty in most of the experimental data is rather large. However, the fact that all experimental relaxation times in this region including the data with higher precision lie above the predicted curve leads us to the conclusion that there exists a discrepancy between theory

TABLE II. The parameters A_1 and A_2 of fitting Eq. (4.2) to the relaxation data of the various Cu-Ni compositions; $T_A = 400$ °C.

Ni (at.%)	30	40	47.5	56.5	60	65	70	80
$A_1(10^{-4})$	12.0	7.7	3.8	4.4	2.2	2.1	1.6	2.8
$A_2(10^{-4})$	8.2	8.5	19.0	12.0	24.0	16.0	9.4	0.1

TABLE III. The parameters A_1 and A_2 of fitting Eq. (4.2) to the relaxation data of the null matrix at various temperatures.

Temperature (°C)	320	340	400	425	450
$A_1(10^{-4})$	0.11	0.27	4.4	11.0	24.0
$A_2(10^{-4})$	0.29	1.4	12.0	52.0	110.0

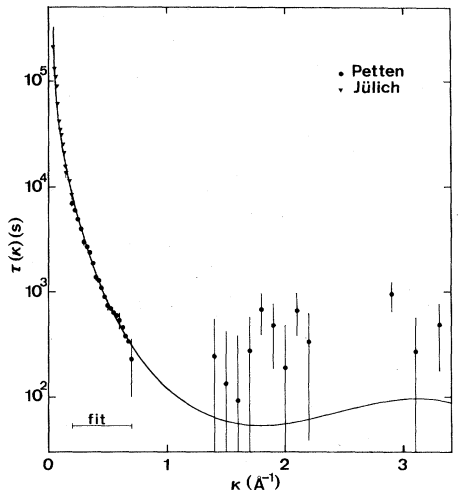

FIG. 7. The relaxation function $\tau(\kappa)$ for the null matrix at 450 °C vs κ. The dots and triangles are the experimental points measured at Petten and at Jülich, respectively. The drawn line is a two-parameter fit of Eq. (4.2) to the experimental points in the range $0.2 < \kappa < 0.8$ Å^{-1}. The parameters used are given in Table III.

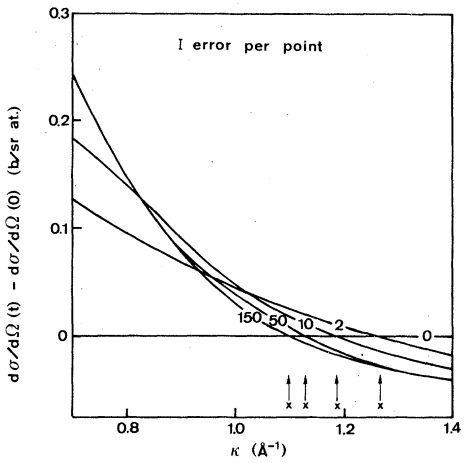

FIG. 8. The gradual shift in the location X of the crossover point with increasing annealing time for the null matrix at 340 °C. The corresponding annealing times (in hours) are indicated in the smoothed lines.

and experiment for large κ values (i.e., short composition wavelengths). This is most likely due to the neglect of multiparticle correlations. As was pointed out by Khachaturyan[5] the relaxation of different wave vectors is independent provided that the three-particle correlation functions can be decoupled. The validity of the decoupling approximation is doubtful for short distances, especially for the CuNi system, for which many-particle interactions are important as follows from the asymmetry of the composition dependence of the clustering parameters.

Two other possible explanations for the discrepancy can be mentioned. Firstly, since we used a polycrystalline sample we measured the time rate of change of the average intensity corresponding to all diffraction vectors $\vec{\kappa}$ with a given length κ. The term $B^2(\vec{\kappa})$ depends on the direction in reciprocal space. Thus both the diffuse intensity and the relaxation time are anisotropic. In general, large relaxation times correspond with high intensities. Hence a spherical average of the relaxation time will underestimate the experimental value. However, since in the range of κ values between 1 and 1.5 Å^{-1} the anisotropy of the term $B^2(\vec{\kappa})$ is fairly small (see Fig. 9), this possibility can be discarded.

Secondly, the presence of elastic anisotropy causes a corresponding anisotropy of the diffuse intensity. The elastic energy contribution to the heat of mixing of CuNi alloys was calculated by Paulson.[30] The calculated values vary from 2 to 4.5×10^8 J m^{-3}. For the same reason as given above, one would expect that in this case the experimental relaxation times would be larger than the theoretical values. To a first approximation the elastic contribution to the free energy is independent of the wavelength of the composition modulation. Thus the anisotropy of the elastic energy would have the same influence at both small and large κ values. It is possible, however, that a more refined model, e.g., the microscopic elasticity theory given by Cook *et al.*,[31] would yield different results in the short-wavelength region.

The ratio of A_1 and A_2 is proportional to the ratio of $f'' + 2\eta^2 Y$ (the sum of the second derivative of the free energy with respect to the concentration and the elastic energy) and K (the gradient-

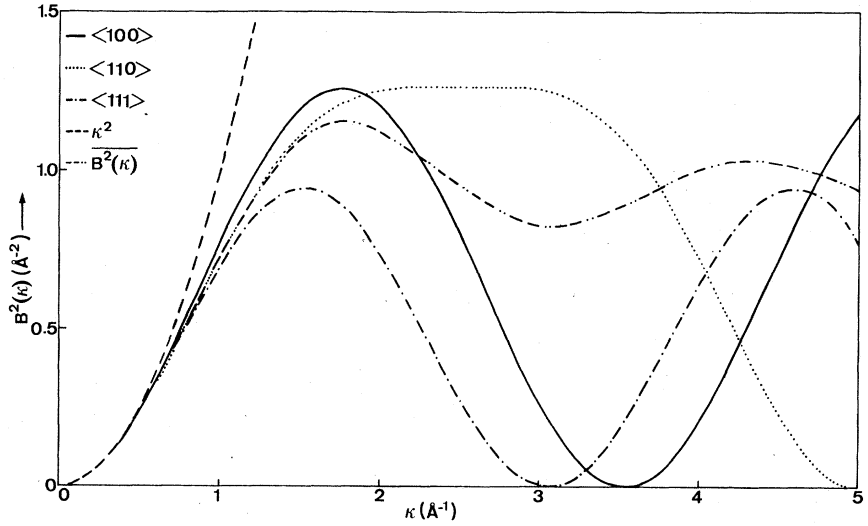

FIG. 9. $B^2(\vec{\kappa})$ as a function of κ for three different directions and the long-wavelength approximation and mean value of $B^2(\vec{\kappa})$.

TABLE IV. The ratio of $f''+2\eta^2 Y$ (the second derivative of the free energy with respect to the concentration and the elastic energy) and K (the gradient-energy coefficient) for the null matrix for various temperatures obtained from the time evolution of the diffuse scattering intensity (kinetic) and from its value for the equilibrium state.

Temperature (°C)	$\frac{f''+2\eta^2 Y}{K}$ (10^{20} m^{-2}) equil.	$\frac{f''+2\eta^2 Y}{K}$ (10^{20} m^{-2}) kinetic
320		0.72
340		0.37
400	0.68	0.70
425	0.70	0.40
450	0.76	0.41
500	0.94	
600	1.43	
700	1.61	

energy coefficient). As explained in the Introduction, this ratio can also be determined from measurements of the diffuse-scattering intensity of the equilibrium state. A comparison between the kinetic and equilibrium results for the null matrix is given in Table IV and for the other compositions in Table V. Agreement is quite reasonable, especially if one keeps in mind that the use of the fluctuation formula (2.8) is not quite justified at temperatures close to the miscibility gap.

The two parameters A_1 and A_2 obtained from fitting Eq. (4.2) to the experimental $\tau(\kappa)$ contain three independent variables, the chemical diffusion coefficient $\tilde{D}$, the gradient-energy coefficient K, and $f''+2\eta^2 Y$, the sum of the second derivative of the local free energy $f(c,T)$ with respect to the concentration and the elastic energy. Hence, additional information on at least one of these three parameters is necessary. Tracer diffusion coefficients of Cu and Ni have been measured by Monma *et al.*[32] at high temperatures (above 900 °C). These data must be extrapolated over about 10 orders of magnitude. This and the few compositions for which the tracer diffusion coefficients have been determined make $\tilde{D}$ less suitable to use as an input parameter. The concentration gradient-energy coefficient K is not very useful either, since K is a complicated function of interaction range and interaction potentials. Fortunately $f''+2\eta^2 Y$ can be determined from thermodynamic data and elastic constants with greater accuracy. The results of measurements of thermodynamic properties have been summarized in Refs. 33 and 34. We used the so-called subregular approximation with a critical temperature of 250 °C at 68 at.% Ni. The calculated values for $f''+2\eta^2 Y$ at 400 °C are given in Table VI which also gives the values of K and $\tilde{D}$ which were calculated from A_1 and A_2 using these values of $f''+2\eta^2 Y$. The calculated values for the null matrix at different temperatures are given in Table VII.

The values of the chemical diffusion coefficients $\tilde{D}$ at 400 °C are plotted as a function of composition in Fig. 10. Also shown are the extrapolated values of $\tilde{D}$ obtained from the tracer diffusion coefficients of Cu and Ni measured by Monma *et al.*[32] and Anusavice *et al.*[35] The agreement between our results and the high-temperature data is good considering the fact that the high-temperature data were extrapolated by more than 10 orders of magnitude. Figure 10 also shows some of the data obtained by Paulson[30] who measured the homogenization of composition-modulated CuNi specimens by means of resistivity measurements. The concentration dependence of the chemical diffusion coefficient is less than, e.g., that of the self-diffusion coefficient of Cu which changes about two orders of magnitude when going from pure Cu to pure Ni.

TABLE V. The ratio of $f''+2\eta^2 Y$ (the second derivative of the free energy with respect to the concentration and the elastic energy) and K (the gradient-energy coefficient) at 400 °C for various compositions obtained from the time evolution of the diffuse scattering intensity (kinetic) and from its value for the equilibrium state.

Ni (at.%)	30	40	47.5	56.5	60	65	70	80
$\frac{f''+2\eta^2 Y}{K}$ (10^{20} m^{-2}) equil.		2.37	1.04	0.68	0.63	0.49	0.56	1.1
$\frac{f''+2\eta^2 Y}{K}$ (10^{20} m^{-2}) kinetic	2.74	1.71	0.38	0.70	0.17	0.25	0.33	54.0

TABLE VI. The gradient-energy coefficients K and the chemical diffusion coefficients $\tilde{D}$ for various compositions at 400 °C deduced from the kinetic parameters A_1 and A_2 of Table II, using values of f'' calculated with the so-called subregular approximation. The elastic energy $2\eta^2 Y$ calculated by Paulson (Ref. 30) was used. Also given are the values of K_1 and K_{1+2} which were calculated from pair interaction potentials for nearest neighbors and for nearest- and second-nearest neighbors obtained from measurements at the equilibrium state (Refs. 20, 22).

Ni (at.%)	30	40	47.5	56.5	60	65	70	80
$K(10^{-11}\ \mathrm{J\,m^{-1}})$	1.15	1.29	4.50	1.88	6.96	4.62	3.76	0.04
$K_1(10^{-11}\ \mathrm{J\,m^{-1}})$	1.79	1.91	1.65	1.70	1.65	1.75	1.86	2.12
$K_{1+2}(10^{-11}\ \mathrm{J\,m^{-1}})$	0.94	0.91	1.04	1.30	1.47	1.43	1.47	1.21
$\tilde{D}(10^{-25}\ \mathrm{m^2\,s^{-1}})$	78.6	63.6	38.9	59.6	32.9	34.8	27.3	38.9
$f''+2\eta^2 Y(10^9\ \mathrm{J\,m^{-3}})$	3.15	2.19	1.71	1.32	1.22	1.17	1.23	1.97

A similar small concentration dependence was also found for the average relaxation time for clustering by van Royen *et al.*[19] who studied the clustering kinetics by means of resistivity measurements.

The temperature dependence of $\tilde{D}$ for the null matrix is presented in Fig. 11, which also shows the extrapolated tracer diffusion data for the $Cu_{0.45}Ni_{0.55}$ alloy[32] and the low-temperature diffusion data of Ref. 36. Our data are in fair agreement with the high-temperature diffusion data. However, the activation energy of the interdiffusion coefficient $\tilde{D}$ [$Q(\tilde{D}) = 1.5 \pm 0.3$ eV] is considerably lower than the activation energies for self diffusion of Cu and Ni ($Q_{Cu} = 2.6 \pm 0.1$ eV and $Q_{Ni} = 2.9 \pm 0.07$ eV). In general one finds a lower activation energy for low-temperature diffusion-controlled processes (kinetics of short-range order, Zener relaxation, etc.) but the differences are usually of the order of 20%. The low value found in our case is most likely due to the use of the subregular approximation for the calculation of f''. The variation of f'' with temperature for a given value of the critical temperature is less rapid if one uses a more sophisticated statistical model. Since the constant A_1 contains the product of $f''+2\eta^2 Y$ and $\tilde{D}$, the use of a higher-order approximation will result in an increase in the temperature dependence of $\tilde{D}$ and hence a higher activation energy.

TABLE VII. K, K_1, K_{1+2}, $\tilde{D}$, and $f''+2\eta^2 Y$ for the null matrix at various temperatures. Further details similar to Table VI.

Temperature (°C)	320	340	400	425	450
$K(10^{-11}\ \mathrm{J\,m^{-1}})$	1.27	2.75	1.88	3.57	3.77
$K_1(10^{-11}\ \mathrm{J\,m^{-1}})$		1.90	1.70	1.70	1.70
$K_{1+2}(10^{-11}\ \mathrm{J\,m^{-1}})$		1.18	1.30	1.33	1.33
$\tilde{D}(10^{-25}\ \mathrm{m^2\,s^{-1}})$	1.89	4.32	59.6	141	293
$f''+2\eta^2 Y(10^9\ \mathrm{J\,m^{-3}})$	0.91	1.01	1.32	1.44	1.56

The values of the gradient-energy coefficient K obtained from the various relaxation experiments are given in Tables VI and VII. The gradient-energy coefficient can also be calculated from the pair-interaction potentials. Using the pair-interaction energies obtained from our earlier measurements of the equilibrium amount of clustering[22] we calculated K for nearest-neighbor interaction only:

$$K_1 = -2V_1 r_1^2 ,$$

where r_1 is the interatomic distance, and for both nearest- and second-nearest-neighbor interactions:

$$K_{1+2} = -(2V_1 + V_2) r_1^2 .$$

The calculated values are given in Tables VI and VII and show reasonable agreement with the experimental results.

It is obvious that the quantitative evaluation of

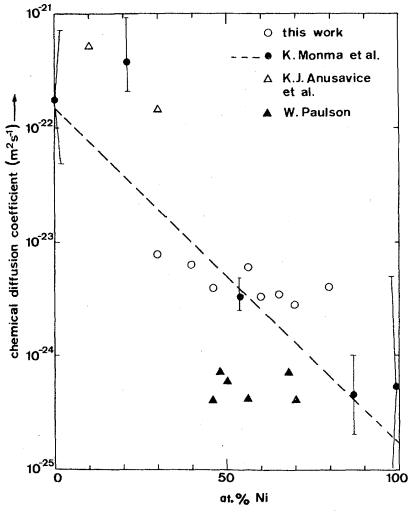

FIG. 10. The chemical diffusion coefficient $\tilde{D}$ of CuNi at 400 °C as a function of composition. The dashed line only serves as a guide for the eye.

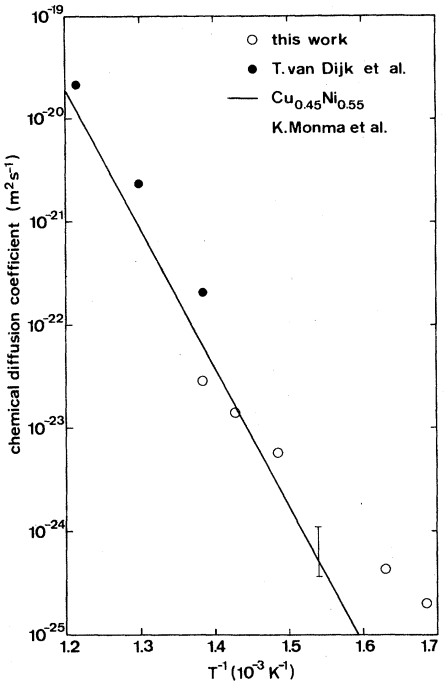

FIG. 11. The chemical diffusion coefficient $\tilde{D}$ of CuNi for the null matrix as a function of T^{-1}.

our results, at least in so far as the numerical values of $\tilde{D}$ and K are concerned, depends rather critically on the concentration and temperature dependence of f''. Admittedly the subregular solution approximation, which hinges on the use of the ideal entropy of mixing, is rather crude. However, the spinodal curve calculated with the use of the subregular approximation and the spinodal determined from the extrapolation of Eq. (2.9) to $\kappa_c^2 = 0$, show good agreement. Moreover, the constants chosen for the subregular approximation are compatible with thermodynamic data.[34]

The use of higher-order approximations for the entropy of mixing is hampered by the fact that the clustering in the CuNi system is rather asymmetric. Moreover, as expected, the asymmetry increases with decreasing temperature. Note that because of the asymmetry many-particle interactions have to be used, since pair interactions will yield a symmetric phase diagram. Many-particle interactions can only be handled in one or another of higher-order approximations, e.g., Kikuchi's cluster variation method.

To conclude our discussion we would like to make some remarks about the relevance of computer simulations[37,38] of spinodal decomposition for the understanding of the phenomena in real systems. Our results on the kinetics of clustering (Fig. 6) show a remarkable similarity to the results of computer simulations. However, our data were obtained above the miscibility gap. The important point is that the wavelengths of the composition modulations in real clustering systems are already larger than the size of the computer models used. For example, in the 450-°C relaxations, the peak in the intensity after 32 h corresponds with a wavelength of 60 Å (17 unit cells), i.e., about twice the size of the usual computer model. This indicates that for practically useful simulations much larger models have to be used. Perhaps a more promising approach is the cluster dynamics model proposed by Binder and coworkers.[39-41] Unfortunately, to our knowledge the theory has been applied so far only to rather dilute alloys (≃20 at.% solute) for which systems percolation (i.e., the appearance of clusters of infinite size) does not occur.

Another problem is that it will be very difficult to distinguish experimentally between spinodal decomposition and clustering which will always precede or accompany the decomposition process. Perhaps a proper distinction is only possible deep inside the spinodal region where the wavelength with the highest growth rate will be comparatively short.

VI. CONCLUSIONS

Cook's theory of the kinetics of clustering based on the discrete lattice diffusion theory of Cook, de Fontaine, and Hilliard gives a good description of clustering kinetics for scattering vectors up to $\simeq 0.8$ Å^{-1} (corresponding to composition wavelengths of $\simeq 8$ Å). However, owing to the assumption that composition waves grow or decay independently, the theory does not correctly describe the behavior near the crossover point.

The values of the diffusion coefficient $\tilde{D}$ are in good agreement with extrapolated high-temperature diffusion data. Also the values of the gradient-energy coefficients K agree well with theoretical calculations using pair-interaction energies obtained from our equilibrium clustering measurements.

ACKNOWLEDGMENTS

Special thanks are due to Professor W. Schmatz, Dr. J. Schelten, and Dr. D. Schwahn of the Kernforschungsanlage Jülich for putting their facilities at our disposal and for their cooperation.

We gratefully acknowledge Mr. H. J. Bron of the Laboratorium voor Fysische Metaalkunde, Rijksuniversiteit Groningen for his cooperation in preparing the specimens and Mr. W. van der Gaauw for his technical assistance in the experiments at Petten. The FOM (Stichting Fundamenteel Onderzoek der Materie) sponsored this work with a grant for the isotopes.

*Present address: Neratoom, The Hague, The Netherlands.
[1]S. Radelaar, Phys. Status Solidi 27, 1163 (1968).
[2]S. Radelaar and J. M. J. Ritzen, Phys. Status Solidi 31, 277 (1969).
[3]S. Radelaar, J. Phys. Chem. Solids 31, 219 (1970).
[4]H. E. Cook, J. Phys. Chem. Solids 30, 2427 (1969).
[5]A. G. Khachaturyan, Fiz. Tverd. Tela (Leningrad) 9, 2594 (1967) [Sov. Phys. Solid State 9, 2040 (1968)].
[6]A. G. Khachaturyan, Fiz. Tverd. Tela (Leningrad) 11, 3534 (1969) [Sov. Phys. Solid State 11, 2959 (1970)].
[7]H. Yamauchi, thesis, Northwestern University, 1973 (unpublished).
[8]H. E. Cook, Acta Metall. 18, 297 (1970).
[9]H. E. Cook, D. de Fontaine, and J. E. Hilliard, Acta Metall. 17, 765 (1969).
[10]J. W. Cahn and J. E. Hilliard, J. Chem. Phys. 28, 258 (1958).
[11]J. W. Cahn, Acta Metall. 9, 795 (1961).
[12]J. W. Cahn, Acta Metall. 10, 179 (1962).
[13]J. W. Cahn, Acta Metall. 14, 1685 (1966).
[14]J. W. Cahn, Trans. Metall. Soc. AIME 242, 166 (1968).
[15]J. S. Langer, Acta Metall. 21, 1649 (1973).
[16]J. S. Langer, Ann. Phys. (N. Y.) 65, 53 (1971).
[17]J. S. Langer and M. Bar-on, Ann. Phys. (N.Y.) 78, 421 (1973).
[18]D. de Fontaine, in *Treatise on Solid State Chemistry*, edited by N. B. Hannay (Plenum, New York, 1975), p. 129.
[19]E. W. van Royen, G. Brandsma, A. L. Mulder, and S. Radelaar, Scr. Metall. 7, 1125 (1973).
[20]J. Vrijen, thesis, Utrecht, 1977 (unpublished); also Netherlands Energy Research Foundation ECN, Petten (N.H.), Report No. ECN 31, 1977 (unpublished).
[21]J. Vrijen, E. W. van Royen, D. W. Hoffman, and S. Radelaar, J. Phys. (Paris), Colloq. C7, 187 (1977).
[22]J. Vrijen and S. Radelaar, Phys. Rev. B 17, 409 (1978).
[23]G. F. Neilson, Phys. Chem. Glasses 10, 54 (1969).
[24]R. J. Acuña and A. F. Bonfiglioli, Acta Metall. 22, 399 (1974).
[25]M. A. Krivoglaz, *Theory of X-ray and Thermal Neutron Scattering in Real Crystals* (Plenum, New York, 1969).
[26]J. Andries, W. G. Boon, and S. Radelaar, Phys. Lett. 38A, 459 (1972).
[27]J. Bergsma and C. van Dijk, Nucl. Instrum. Methods 51, 121 (1967).
[28]W. Schmatz and J. Schelten, J. Appl. Crystallogr. 4, 410 (1971).
[29]J. Schelten, Kerntechnik 14, 86 (1972).
[30]W. M. Paulson, thesis, Northwestern University, 1972 (unpublished).
[31]H. E. Cook and D. de Fontaine, Acta Metall. 17, 915 (1969).
[32]K. Monma, H. Suto, and H. Oikawa, J. Jpn. Inst. Met. 28, 192 (1964).
[33]L. Elford, F. Müller, and O. Kubaschewski, Ber. Bunsenges. Phys. Chem. 73, 601 (1969).
[34]R. Hultgren, R. L. Orr, P. D. Andersen, and K. K. Kelley, *Selected Values of Thermodynamics Properties* (American Society for Metals, Cleveland, Ohio, 1973).
[35]K. J. Anusavice and R. T. Detloff, Metall. Trans. 3, 1279 (1972).
[36]T. van Dijk and E. J. Mittemeijer, Thin Solid Films 41, 173 (1977).
[37]J. Marro, A. B. Bortz, M. H. Kalos, and J. L. Lebowitz, Phys. Rev. B 12, 2000 (1975).
[38]A. Sur, J. L. Lebowitz, J. Marro, and M. H. Kalos, Phys. Rev. B 15, 3014 (1977).
[39]P. Mirold and K. Binder, Acta Metall. 25, 1435 (1977).
[40]K. Binder, D. Stauffer, and H. Müller-Krumbhaar, Phys. Rev. B 12, 5261 (1975).
[41]K. Binder, Phys. Rev. B 15, 4425 (1977).